Structural basis for the efficient phosphorylation of AZTMP and dGMP by Plasmodium falciparum type I thymidylate kinase.

Jean L Whittingham, Juana Carrero-Lerida, Jim A Brannigan, Luis M. Ruiz-Pérez, Ana P.G. Silva, Mark J. Fogg, Anthony J Wilkinson, Ian H. Gilbert, Keith S Wilson, Dolores González-Pacanowska

Structural basis for the efficient phosphorylation of AZTMP and dGMP by *Plasmodium falciparum* type I thymidylate kinase.

Jean L. WHITTINGHAM*[2], Juana CARRERO-LERIDA†[2], James A. BRANNIGAN*, Luis M. RUIZ-PEREZ†, Ana P. G. SILVA*, Mark J. FOGG*, Anthony J. WILKINSON*, Ian H. GILBERT‡, Keith S. WILSON*[1] & Dolores GONZÁLEZ-PACANOWSKA†[1]

*Structural Biology Laboratory, Department of Chemistry, University of York, Heslington, York YO10 5YW, UK

†Instituto de Parasitología y Biomedicina "López-Neyra", Consejo Superior de Investigaciones Científicas, Parque Tecnológico de Ciencias de la Salud, Avenida del Conocimiento s/n, 18100-Armilla, Granada, Spain

‡College of Life Sciences, University of Dundee, Sir James Black Centre, Dundee DD1 5EH, Scotland, UK

[1]Correspondence may be addressed to either Dolores González-Pacanowska (e-mail dgonzalez@ipb.csic.es) or Keith Wilson (e-mail keith@ysbl.york.ac.uk).

[2]These authors contributed equally to this work.

Key words: malaria, thymidylate kinase, ligand complexes, structure, kinetics, drug target.

Abbreviations used: AP_5dT, P^1-(5'-adenosyl)-P^5-(5'-thymidyl) pentaphosphate; AZTMP, 3'-azido-3'-deoxythymidine monophosphate; DTT, 1,4-dithio-DL-threitol; 5FdUMP, 5-fluoro-2′-deoxyuridine-5′-monophosphate; hTMPK, human thymidylate kinase; *Pf*TMPK, *Plasmodium falciparum* thymidylate kinase; rmsΔ, root mean square positional deviation; TMPK, thymidylate kinase.

SYNOPSIS

Plasmodium falciparum is the causative agent of malaria, a disease where new drug targets are required due to increasing resistance to current anti-malarials. Thymidylate kinase (TMPK) is a good candidate since it is essential for the synthesis of dTTP, a critical precursor of DNA and has been much studied due to its role in prodrug activation and as a drug target. Type I TMPKs such as the human enzyme, phosphorylate the substrate 3'-azido-3'-deoxythymidine monophosphate (AZTMP) inefficiently compared to type II TMPKs (e.g. *E. coli* TMPK). Here we report that eukaryotic *P. falciparum* TMPK presents sequence features of a type I enzyme yet kinetic parameters for AZTMP phosphorylation are similar to those of the highly efficient *E. coli* enzyme. Structural information shows that this is explained by a different juxtaposition of the P-loop and the azide of AZTMP. Subsequent formation of the transition state requires no further movement of the *Pf*TMPK P-loop, with no steric conflicts for the azide moiety, allowing efficient phosphate transfer. Likewise, we present data that confirm the ability of the enzyme to accept uniquely dGMP as a substrate and sheds light on the basis for its wider substrate specificity. Information resulting from two ternary complexes (dTMP-ADP and AZTMP-ADP) and a binary complex with the transition state analogue P^1-(5'-adenosyl)-P^5-(5'-thymidyl) pentaphosphate all reveal significant differences with the human enzyme notably in the lid region and in the P-loop which may be exploited in the rational design of *Plasmodium*-specific TMPK inhibitors with therapeutic potential.

INTRODUCTION

An essential step in the biosynthesis of the nucleotide dTTP is the phosphorylation of dTMP to dTDP. This reaction is catalysed by thymidylate kinase (TMPK, EC 2.7.4.9, ATP:dTMP phosphotransferase) in a magnesium-dependent manner with ATP as the preferred phosphate donor. Cellular production of dTTP is a highly regulated process [1, 2] that is coordinated with DNA replication in the cell cycle and TMPK has a central role in the control of the dTTP pool size in eukaryotic cells. The enzyme has been widely studied partly owing to its participation in the pathway that leads to the activation of a number of pro-drugs, including azidothymidine (AZT) and acyclovir for the treatment of AIDS and herpes simplex virus infections, respectively [3, 4]. TMPK is also being investigated as a drug target in its own right and specific inhibitors of the orthologous enzymes from *Bacillus anthracis* and *Mycobacterium tuberculosis* have been developed [5, 6].

TMPK is found in all organisms requiring *de novo* pyrimidine synthesis, and crystal structures of the enzyme from a number of different species have been determined [7-11]. The protein is a homodimer with a subunit fold consisting of a five-stranded parallel β-sheet surrounded by 7-11 α-helices. The nucleotide substrates are bound in a groove on the surface of the subunit which is characterised by a number of conserved sequence motifs containing structural elements required for substrate recognition and catalysis, namely the so-called 'P-loop' [12], $G(X)_4GKS/T$, the critical loop DRX motif (Figure 1a) and a 'lid' that partially encloses the phosphate donor and is implicated in catalysis [8]. Crystal structures of TMPKs with different combinations of ligands have revealed several conformational states of the protein: an open state in the absence of ligand (where the lid is disordered); a partially closed state in the presence of dTMP (lid disordered in most structures, but ordered in the *M. tuberculosis* enzyme); and a fully closed state in the presence of both co-substrates (lid ordered). Co-crystallisation with bi-substrate analogues such as P^1-(5'-adenosyl)-P^5-(5'-thymidyl) pentaphosphate (AP_5dT), which mimic the ATP-dTMP or ADP-dTDP states [13] has given additional insight into the reaction coordinate [14, 15].

After extensive functional and structural studies on TMPK from several species, a general consensus with regard to the mechanism has been achieved. There is a good overview of the mechanism based primarily on structural and functional studies of the human enzyme [15]. Due to the complexity of the reaction, there are small differences between species, such as the movement of the P-loop and the lid during catalysis so as to re-orient specific basic side chains to stabilise the transition state complex. These may well have impacts on the specificity and relative kinetics of the enzyme. Sequence variation, particularly in the lid region, is associated with structural alterations around the nucleotide-binding site and relocation of catalytic side chains, leading to speculation that the subtleties of the mechanism vary between species [8]. Comparison with related systems has given some general insights into the mechanism. In a similar fashion to adenylate kinase, which has the same overall topology as TMPK, the two nucleotide substrates are believed to bind to the enzyme via a random bi-bi mechanism [16]. It is agreed that phosphate transfer occurs via an associative, rather than a dissociative, mechanism such that the migrating phosphate is bound to both substrates in the transition state [17]. The accumulating negative charge on this phosphate in the transition state is proposed to be stabilised by arginine side chains and one or more magnesium ions.

The TMPKs have been classified into two groups [8]. Type I enzymes, which include the human, yeast and *Plasmodium* proteins, have a basic residue in addition to the lysine in the P-

loop (Arg^{18} in *Pf*TMPK). Type II enzymes including that from *Escherichia coli*, lack this basic residue in the P-loop; alternatively a basic residue from the lid appears to exert a similar function. TMPKs from different species have varying 3'-azido-3'-deoxythymidine monophosphate (AZTMP) phosphorylation efficiencies and comparative structural and biochemical studies have shown the structural basis for proficient phosphorylation. TMPKs from *E. coli* and various viruses are able to phosphorylate AZTMP very much more efficiently than the human enzyme [18]. The reason for this appears to be the displacement of a catalytically important arginine side chain on the P-loop of the human enzyme in response to AZTMP binding. In contrast the *E. coli* enzyme, where the P-loop arginine is absent, can accommodate AZTMP without seriously affecting its catalytic properties [8].

The focus of the present study is to explore the potential of *P. falciparum* TMPK (*Pf*TMPK) as an anti-malarial drug target. We present a kinetic analysis of *Pf*TMPK in combination with the crystal structure of four ligand complexes: dTMP-ADP, AZTMP-ADP, AP_5dT and dGMP-ADP. The latter structure provides a structural rationalisation for the broader specificity of the *Plasmodium* enzyme. Two recent studies by Kitade and colleagues presenting results on the expression and kinetics [19] and on the ligand binding, modelling and mutagenesis [20] of *Pf*TMPK, together with new kinetic data are interpreted in terms of the crystal structures presented herein. The present results confirm that the enzyme has structural and catalytic properties distinct from other members of the family, confirming that it is a good candidate for selective inhibition and rational drug design.

EXPERIMENTAL

Materials

AZTMP, 3'-dGMP and AP_5dT were purchased from Jena Biosciences GmbH. Other nucleotides including ATP (magnesium salt) were purchased from Sigma-Aldrich Company Ltd. Oligonucleotides were synthesized at the Analytical Services of the López-Neyra Institute of Parasitology and Biomedicine. *P. falciparum* strain 3D7 was provided by J. M. Bautista of the University Complutense of Madrid (Spain). Human erythrocytes and frozen serum were obtained from Centro Regional de Transfusión Sanguínea-SAS (Granada, Spain).

Parasite culture

P. falciparum strain 3D7 was cultured by the method of Trager and Jensen [21] with minor modifications. Cultures were maintained in fresh group O-positive human erythrocytes suspended at 5% hematocrit in RPMI 1640 (GibcoBRL) containing 10% human serum, 3 g glucose, 45 µg hypoxanthine, and 50 µg of gentamicin per liter. The medium was changed daily, as previously described [21].

Expression of *Pf*TMPK in *Escherichia coli*

DNA encoding full length *Pf*TMPK (633 bp) was amplified by RT-PCR from total RNA obtained by standard procedures from parasites released from infected erythrocytes by saponin lysis [22]. The primer TKEcoRI (5'-GGAATTCTTATGACCACAAAAAATTAA-3') was used to synthesize the corresponding *tmpk* cDNA, in the reverse transcriptase reaction, and TKNdeI (5'-GCATATGACTGATGATAAAAAAAA-3') and TKEcoRI were used in a second PCR step to amplify the full coding sequence with *Nde*I and *EcoR*I restriction sites placed at the 5' and 3' ends respectively for cloning into the plasmid vector pET28a (Novagen) so as to append a His_6-affinity purification tag and a thrombin cleavage site to the N-terminus of the *Pf*TMPK peptide sequence. The resulting pET-*Pf*TMPK plasmid was used to transform the *E. coli* strain BL21 (DE3) and *Pf*TMPK expression was induced by adding 1 mM isopropyl β-D-thiogalactoside (Roche) and incubating for 4 h at 37ºC or by means of auto-induction [23] for a period of 20 h. The cultures were collected by centrifugation and frozen at -80ºC until use.

Purification of recombinant *Pf*TMPK

For purification of *Pf*TMPK, cell pellets were resuspended in 10 ml of binding buffer (50 mM Tris-HCl pH 7.5, 300 mM NaCl, 10 mM imidazole, 1 mM DTT) and protease inhibitor cocktail (Pefabloc SC, Roche Diagnostics GmbH) to a final concentration of 2 mM. PSC-protector solution was also added to prevent non-specific covalent attachment of the protease inhibitor to the protein (a problem encountered during initial purification trials). Cells were disrupted by sonication on ice and centrifuged at high speed for 30 min at 4ºC. The cleared lysate was applied to a HiTrap Chelating HP affinity column (Amersham Biosciences) equilibrated with binding buffer. The column was washed with binding buffer containing 20 mM imidazole, and was developed with a linear gradient of 20 to 500 mM imidazole. Fractions containing the enzyme were pooled, passed through a PD-10 column (GE Healthcare) and eluted in 50 mM Tris-HCl pH 7.5, 20 mM NaCl, 1 mM DTT and 50% glycerol. For structural work, the protein was further purified by gel filtration on a HiLoad

16/60 Superdex 75 prep-grade gel-filtration column (Amersham Biosciences) pre-equilibrated with 50 mM Tris-HCl pH 8.5 and 200 mM NaCl. Protein concentration was determined by the method of Bradford [24], with bovine serum albumin as a protein standard. The purity and molecular mass of the purified protein were established by polyacrylamide gel electrophoresis and electrospray mass spectrometry. The protein was concentrated to 40 mg ml^{-1} and stored at -80º C.

Activity assays

Recombinant *Pf*TMPK enzyme activity was assayed using a spectrophotometric method by coupling the formation of ADP to the oxidation of NADH in reactions catalyzed by pyruvate kinase and lactate dehydrogenase [25]. Assays for inhibition determination were performed in a final volume of 1 ml and a standard assay contained 50 mM Tris-HCl (pH 7.4), 50 mM KCl, 5 mM $MgCl_2$, 0.2 mM NADH, 1 mM DTT, 1 mM phosphoenolpyruvate, pyruvate kinase (4 U), lactate dehydrogenase (4 U), 50 µM dTMP, 1 mM ATP and 0.83 µg of recombinant enzyme. When K_m and V_{max} values for the different nucleotides were determined, a range of concentrations were tested using the standard assay. TMPK activity (1 unit) was defined as that which produces 1 nmol of NAD^+ per minute and mg of enzyme. K_i values were obtained from the expression $I50 = K_i\,(1+[S]/K_m)$ that, for competitive inhibitors, relates the concentration of inhibitor which inhibits activity by 50% (I50) with the K_i value. K_m is the Michaelis-Menten constant for dTMP and [S] is the concentration of dTMP used in the reaction (50 µM).

Crystallisation, data collection and data processing

To remove the His_6-tag from the protein prior to crystallisation, biotinylated thrombin (Novagen) was added to a solution containing 1 mg ml^{-1} *Pf*TMPK in 50 mM Tris-HCl pH 8.5, 200 mM NaCl and 2.5 mM $CaCl_2$ (1 unit of thrombin per µg of protein). This solution was gently swirled at room temperature for 24 h. The thrombin was then removed from the reaction mix by immobilisation on streptavidin agarose according to the manufacturer's instructions, and a final nickel affinity chromatography step was used to remove any uncleaved *Pf*TMPK. Electrospray mass spectrometric analysis confirmed the identity and purity of the product and the presence of a Gly-Ser-His extension at the N-terminus of the protein (24,973 kDa). Needle-shaped crystals (up to 50 x 50 x 400 μm^3 in size) of four different nucleotide complexes of *Pf*TMPK were obtained using hanging drop vapour diffusion, with a 1:1 mixture of protein solution and reservoir solution in the drop (see Supplementary Table). Prior to data collection, the crystals were vitrified at 120 K in an appropriate cryoprotectant solution (see Supplementary Table). X-ray data sets for the four protein complexes (Table 3) collected at the ESRF in Grenoble, were processed using DENZO and SCALEPACK [26]. Initial data on the dGMP complex were collected on the ID24 microfocus beam line at the Diamond Light Source from a crystal conglomerate using a 8x8 µm beam to hunt for a single lattice with the help of Gwyndaf Evans, Robin Owen and Danny Axford. This led to a 70 % complete data set at 2.7 Å resolution and allowed the presence of the ligand to be confirmed. While subsequent optimisation led to larger crystals from which complete data were recorded at the ESRF, the power of beam line I24 for analysing tiny crystals was clearly demonstrated by this result.

Structure solution and refinement

The structure of *Pf*TMPK complexed with dTMP and ADP was solved by molecular replacement with the program PHASER [27] using human TMPK (pdb code 1e2q) as a search model (the two proteins share 39% sequence identity). Searches, carried out in two possible space groups ($P3_121$ and $P3_221$), yielded solutions in space group $P3_121$ only and established the presence of three molecules per asymmetric unit. Refinement was carried out in the CCP4 suite of programs [28] using maximum likelihood methods implemented in REFMAC [29]. 5% of the data were excluded for *R*-free calculations. The models were manually rebuilt using the program COOT [30] in conjunction with a 3-fold averaged $2F_o$-F_c electron density map and a F_o-F_c electron density map. After several rounds of refinement and model building, the dTMP and ADP molecules were built into electron density in the averaged map. Towards the end of the refinement small differences between the three molecules were modelled into a non-averaged $2F_o$-F_c electron density map and two metal ions were located in each of the three molecules. The other three protein complexes were refined starting from the dTMP-ADP complex without its solvent and ligands and rebuilt in a similar manner. Dictionaries for the nucleotide ligands were made using PRODRG [31]. Refinement statistics and structural information are listed in Table 3.

Protein Data Bank accession numbers

The atomic coordinates and structure factors for the four *Pf*TMPK complexes have been deposited in the Protein Data Bank, www.ebi.ac.uk (ID codes: dTMP-ADP: 2wwf, dGMP-ADP: 2wwg, AP_5dT: 2wwh and AZTMP-ADP: 2wwi).

RESULTS AND DISCUSSION

Kinetic parameters and inhibition of *Pf*TMPK

Standard procedures were used to determine the kinetic parameters of recombinant *Pf*TMPK. Plots of specific activity versus substrate concentration gave typical Michaelis-Menten hyperbolic saturation curves. Kinetic constants were determined for a number of different substrates used as phosphoacceptors (Table 1). ATP was used as a phosphate donor in the assays, because it was the preferred donor among those tested (results not shown). The phosphorylating efficiency (k_{cat}/K_m) of *Pf*TMPK was highest for dTMP followed by dGMP, 5FdUMP, dUMP, dIMP and GMP. In addition the K_m for ATP was 78.6 μM. This value was obtained at 200 μM dTMP and constant free Mg^{2+} concentrations (5 mM). These results are in general agreement with those previously reported [19], with the relative activities having the same rank order although the two assays differ in the absolute measured values. While the assay methodology used in both cases is similar, subtle differences may be due to the different expression systems employed or minor differences in the reaction conditions. It is of particular note that the activity is almost as high for the purine dGMP as it is for dTMP. Surprisingly, phosphorylation of the nucleotide analogue AZTMP was also highly efficient with k_{cat}/K_m close to half that for dTMP. This latter value for AZTMP is 200-fold higher than the corresponding value for human TMPK (henceforth hTMPK) and similar to that of the *E. coli* enzyme (Table 2).

There was no measurable phosphorylation of the nucleosides uridine, thymidine, deoxyuridine, and AZT by *Pf*TMPK. Likewise, purine derivatives such as ganciclovir (9-[(1,3-dihydroxy-2-propoxy) methyl] guanine) and 3'-deoxyguanosine-5'-monophosphate were not substrates. Different nucleotides and nucleosides were tested as inhibitors of dTMP phosphorylation. 5-fluoro-2'-deoxyuridine and 3'-deoxyguanosine-5'-monophosphate showed K_i values of 1.6 mM and 0.25 mM respectively while no inhibition was observed with deoxyuridine, 5-fluoro-5'-deoxyuridine or ganciclovir. The K_i for AP_5dT, a bi-substrate inhibitor of several thymidylate kinases [13] was measured by determining the percentage of inhibition at different inhibitor concentrations and assuming competitive inhibition, giving a value of 0.31 μM. The key findings of the kinetic studies are the high activity of *Pf*TMPK on AZTMP, and confirmation of its activity on dGMP. These activities will be discussed in terms of the structural investigations below.

The three dimensional structure

*Pf*TMPK is a homodimeric protein containing 210 amino acid residues per subunit. All four nucleotide complexes crystallised in space group $P3_121$ with three protomers per asymmetric unit, equating to one crystallographically independent dimer, plus a second dimer lying on a crystallographic two-fold axis. We first give a generic description of those features which are common to all four complexes, before describing the structures in detail in the subsequent sections.

The three protomers are essentially identical to one another, with root mean square positional deviations (rmsΔ) following superposition of all C_α atoms of ~0.25 Å. Each subunit has a globular structure consisting of a five-stranded parallel β-sheet (β2–β3–β1–β4–β5) surrounded by eight α-helices (Figure 1b). Interaction with the partner subunit in the dimer occurs predominantly through hydrophobic interactions between α-helices 2, 3 and 5 from

each subunit (not shown). The molecules are well-ordered, with only some small loop and chain termini disorder. Superposition of protomer A from all four complexes shows the backbone conformation to be very similar (Supplementary Figure S1) and corresponds to the closed form of the enzyme, as expected for complexes with both nucleotides.

In the dTMP-ADP, AP_5dT and dGMP complexes, there are two peaks at essentially identical positions in the electron density maps adjacent to the terminal phosphate groups of the nucleotides, whose shape and coordination indicated the presence of two metal ions. These were initially introduced as Mg^{2+} ions since magnesium had been included in the crystallisation solutions. However, following refinement, it became clear from the metal-ligand bond distances (2.3 – 2.6 Å) that the ions were in fact sodium. The metal sites are shown for the dTMP-ADP complex in Figures 1b & 2c. The two ions, Na (I) and Na (II), are situated 7.0 Å apart with well-defined and independent coordination spheres. In retrospect, this is not surprising as although 25 mM magnesium chloride was present in the crystallisation drops, sodium is also present at large excess, ~1-2 M. These sodium ions in *Pf*TMPK, primarily due to their larger ionic radius, occupy somewhat different positions to those observed for the "biological" Mg^{2+} ions seen in the human enzyme (Figure 2c), and some other known structures, which correspond to the two metal ions essential for phosphoryl group transfer. Equivalent sodium ions are likely to be present, but were not modelled, in the lower resolution AZTMP complex. The sodium ions have rather different coordination from the magnesium ions, as described in the next section, with bonds formed to the nucleotides and protein residues.

*Pf*TMPK has the same general fold and mode of substrate binding as other TMPKs with known structures (www.ebi.ac.uk), suggesting a common mode of action. Thus, *Pf*TMPK would be expected to bind the two nucleotide co-substrates independently of one another, with binding accompanied by stepwise closure of the P-loop and lid so that phosphate transfer can be facilitated by magnesium ions, arginine side chains, and other essential conserved residues.

A superposition of the dTMP-ADP complex of *Pf*TMPK on the equivalent complex of the human enzyme shows that the cores of the molecules are very similar (see below), with some minor differences evident in the loops remote from the active site, and some significant deviations in the loops close to the active site (Supplementary Figure S2). A set of sub-states of the closed form of the human enzyme, with the lid and P-loop being either in the open, half-closed or closed form depending on the ligand bound have been described [15]. Comparison of the backbone conformation of *Pf*TMPK with that of the human enzyme complexes shows that it corresponds most closely to the closed sub-conformation of the lid and P-loop (Supplementary Figure S3). Indeed in terms of the "degree of closure", *Pf*TMPK appears to be even more tightly closed around the nucleotides in the four complexes than in the equivalent human structures. In all, the comparison of *Pf*TMPK and hTMPK reveals significant and consistent conformational changes in the catalytically important P-loop and lid regions. These conformational differences together with natural side chain variations may account for differences in specificity and rate in the two enzymes.

The *Pf*TMPK-dTMP-ADP complex

The structure of the *Pf*TMPK-dTMP-ADP complex was refined at a resolution of 1.9 Å. A prominent groove on the surface of each subunit forms the binding site for dTMP and the preferred phosphate donor, ATP, which bind co-linearly to facilitate phosphate group transfer. Residues of the lid region flank the bound nucleotides, partially enclosing the binding site.

The presence of both dTMP (substrate) and ADP (product) results, as stated above, in the closed form of the enzyme with the lid fully ordered. The dTMP is buried, the thymine base being maintained in position by hydrogen bonds (both directly and indirectly via ordered water molecules) to the side chains of Arg^{78} and Tyr^{153}, and a ring stacking interaction with Phe^{74} (Figure 2a). The ribose ring is loosely packed between the side chains of Tyr^{153} and Arg^{99}, and forms one direct hydrogen bond to Asp^{17} in the P-loop. There is clear evidence for the binding of two sodium ions (Figure 2c). The phosphate group makes direct interactions with the side chain of Arg^{99} and Na (I) which is penta-coordinate, its ligands consisting of a phosphate oxygen (from dTMP), the side chain oxygen atoms of Asp^{17} and Glu^{154} and two water molecules (Figure 2c). The existence of a third highly mobile water molecule to complete the octahedral coordination sphere cannot be excluded. Arg^{99}, which forms part of the highly conserved critical loop, is the only residue in the structure whose main chain bond angles lie in a disallowed region of the Ramachandran plot. This phenomenon has been observed in other thymidylate kinases, and can be presumed to be associated with catalysis since steric strain in well refined crystal structures correlates with functional significance [32]. The residues involved in dTMP binding are highly conserved and superposition of the dTMP-bound TMPK structures available from the PDB shows that the mode of binding is very similar in each.

The ADP, bound close to the surface of the protein, is protected by the lid and is secured in position by a number of interactions (Figure 2b). These include stacking between the adenine base and the guanidine moiety of Arg^{145}, a hydrogen bond between the base and the main chain oxygen of Arg^{182}, three hydrogen bonds between the phosphate groups and the atoms of residues Lys^{21}, Ser^{22} and Thr^{23} (P-loop), and a direct interaction with the second sodium ion, Na (II). Na (II) has an octahedral coordination sphere comprising a phosphate oxygen from ADP, the side chain carboxylate of Asp^{98}, the side chain oxygen atom of Ser^{19} and three water molecules. The catalytically important Asp^{17} of the P-loop has a full complement of polar interactions, including hydrogen bonds to Tyr^{107} and Gln^{159}. The side chain of the adjacent Arg^{18} points away from the substrate, hydrogen bonding to the side chain of Glu^{154}.

Superposition of the structure of *Pf*TMPK-dTMP-ADP with the equivalent complex of hTMPK (pdb code 1e2d, sequence identity 40%, sequence homology 60%) shows a highly conserved topology (rmsΔ 1.35 Å over 195 C_α atoms) and mode of nucleotide binding (Supplementary Figure S2); the dTMP binding sites are essentially identical. However, there are small but significant differences in the lid regions, which differ in conformation, and in the P-loops, which have a relative displacement of 2.1 – 2.5 Å on main chain atoms and differences in side chain conformations. For the human enzyme, the P-loop displacement results in a shift in position of the phosphate groups of ADP and a different mode of metal binding reflecting the presence of sodium rather than magnesium (Figure 2c). The different conformation for Asp^{15} results in Mg (I) in hTMPK having a quite different coordination sphere, consisting of six water molecules and an indirect rather than direct interaction with dTMP, compared to that of Na (I) in *Pf*TMPK (Figure 2c). A likely reason for the difference in the position of the P-loop is a natural variation in the substrate binding site, Phe^{105} (human) → Tyr^{107} (*Plasmodium*). The tyrosine side chain of *Pf*TMPK forms a hydrogen bond (2.6 Å) with the side chain of Asp^{17}, which helps to tether this catalytically important residue in close proximity to the terminal phosphate groups of the nucleotide co-substrates (Supplementary Figure S4). The phenylalanine in the human enzyme lacks the capacity to do this. There is a tyrosine at this position in yeast TMPK and this residue has been cited as the reason for its enhanced catalytic activity relative to hTMPK [33]. The other P-loop side chain believed to be important for catalysis, Arg^{18} (Arg^{16} in hTMPK), is directed away from the nucleotide binding site in *Pf*TMPK and hTMPK, in both structures making hydrogen bonding interactions with lid residues. Residue Lys^{37} in yeast TPMK corresponds to Arg^{41} and Tyr^{43} in

the human and *P. falciparum* enzymes, respectively (Figure 1a). These natural variations in the substrate binding site may provide scope for the design of selective inhibitors against *Pf*TMPK.

The structural basis for dGMP phosphorylation

In view of the kinetic observation that *Pf*TMPK phosphorylates dGMP with a k_{cat}/K_m value close to that for dTMP, we determined the structure of the dGMP-ADP complex, which was refined to a resolution of 2.4 Å. Two sodium ions were modelled at equivalent positions to those in the dTMP complex, but with reduced electron densities reflecting the lower resolution of the analysis. The purine nucleotide is accommodated in the pyrimidine binding pocket (Figure 3a) with negligible changes in the protein structure compared to the dTMP-ADP structure (rmsΔ 0.25 Å over 209 C_α atoms). The guanine base is coplanar with the dTMP thymine and just requires the displacement of a single highly ordered water molecule, which in the dTMP-ADP complex hydrogen bonds to atom O2 of thymine and the hydroxyl groups of residues Tyr^{153} and Ser^{108}. The ribose and the phosphate groups of dGMP have closely similar conformations and positions to those of dTMP and the ADP binding sites are essentially identical.

The structure of the human dTMP-ADP complex is superimposed on the *Pf*TMPK complex in Figure 3a. From the close similarity of the two structures, it might be expected that the human enzyme would also bind dGMP. However, in spite of the fact that the dTMP binding site of hTMPK is very similar to that of *Pf*TMPK, particularly around the pyrimidine binding pocket, several studies have demonstrated that dGMP is not a substrate for the human enzyme [34-36]. In human cells it appears that a guanylate kinase very efficiently phosphorylates dGMP and GMP [36]. A survey of the *P. falciparum* genome (www.PlasmoDB.org) shows the existence of a guanylate kinase and a UMP-CMP kinase which have potential functions in dGMP phosphorylation, as guanylate kinases are capable of dGMP phosphorylation [37], likewise certain UMP kinases such as that from yeast have been shown to phosphorylate dGMP [38]. A recent study has revealed that the *P. falciparum* guanylate kinase utilizes dGMP with very low specificity, which is of interest in respect of the potential contribution of *Pf*TMPK to cellular dGDP formation and purine nucleotide metabolism in this parasite [39].

Site-directed mutagenesis has been previously used to evaluate the contributions of selected residues to substrate binding and catalysis [20]. The mutation of the conserved Phe^{74}, whose side chain stacks with the thymine base, to an alanine eliminated activity almost entirely. Introduction of individual point mutations between the human and parasite enzymes (Figure 1a) into *Pf*TMPK, S108T, Y43R and Y43L had negligible effects on activity. The structure of *Pf*TMPK reveals that although these residues are close to the active site, they are not directly involved in nucleotide binding. Substitution of Ala^{111} by Lys, resulted in a dramatic reduction in activity of *Pf*TMPK, especially in dGMP phosphorylation. Ala^{111} resides on a seven-residue loop on the outside of the molecule which has quite different conformations in the two enzymes. As a result, Ala^{111} and K^{109}, rather than coinciding, are displaced by 3.7 Å from one another (C_α), and located 10 – 12 Å away from the dTMP ligand exerting no *direct* influence on binding. Indeed the A111K mutation in *Pf*TMPK would be expected to cause a steric clash with the side chain of Tyr^{153} which is in van der Waals' contact with both the base and the sugar of dTMP. Displacement of the tyrosine side chain would be predicted to affect substrate binding, and this would be exacerbated for the larger dGMP, in keeping with the kinetic data.

Vaccinia virus TMPK is also capable of phosphorylating purine nucleotides [34] and recent structural analysis has revealed a dimer arrangement which is orthogonal and not anti-parallel

as in other TMPKs. This unusual subunit tilting is closely correlated with enzyme stability and with the presence of a cavity allowing broader substrate specificity [40]. Apart from *Plasmodium* and vaccinia TMPKs, the only other kinase that is known to handle both dGMP and dTMP is the bacteriophage T4 deoxynucleotide kinase. The structure of the phage enzyme is similar to the fold of the NMP kinases, but with a different dimerisation mode and no apparent conservation of the active site residues [41].

The *Pf*TMPK-AP_5dT complex

The bisubstrate inhibitor AP_5dT [13] has been co-crystallised with TMPK from a number of species [6, 14, 15]. In the *Pf*TMPK complex, AP_5dT is bound at full occupancy with the same mode of binding in all three protomers (Figure 3b). The five phosphate groups of the inhibitor are labelled PA-PE, phosphate PA being closest to the thymidine group. Superposition with the *Pf*TMPK-TMP-ADP complex shows that the effect of bisubstrate binding on the protein conformation is minimal, with rmsΔ for all main chain atoms of 0.3 Å. The adenosine and thymidine moieties of AP_5dT superpose closely with the nucleoside species of ADP and dTMP, as do the phosphates PA, PD and PE with the phosphate of dTMP and the β and α phosphates of ADP respectively. The two bridging phosphate groups of AP_5dT, PB and PC, are bound next to the P-loop, flanked by the two sodium ions. The non-bridging oxygens of all five phosphate groups make polar interactions with Lys^{21}, Ser^{22} (main chain and side chain), Thr^{23} (main chain), Arg^{47} and Arg^{99} or with the metal ions. In addition, the side chain of Arg^{18} has two alternate conformations, one of which hydrogen bonds to a phosphate oxygen of PC. The presence of this interaction is consistent with a role for Arg^{18} in transition state stabilisation, as has been shown for the yeast and human enzymes. Two sodium ions were modelled in the structure, and lie roughly 0.7 Å from the equivalent ions in the dTMP-ADP complex.

Superposition of *Pf*TMPK-AP_5dT with the equivalent complexes from other species (Figure 3b) confirms that the inhibitors bind in the same place, although only the thymidine moieties are truly coincident. The atoms of the five phosphate groups and the adenosine moieties are displaced by 0.3 – 1.2 Å (one of the phosphates is ordered in the human complex). The Na (I) and Mg (I) ions lie 2.1 Å apart in the human and *Plasmodium* enzymes, although they carry out the same role, coordinating to two oxygen atoms of phosphates PC and PD (by *Pf*TMPK naming of phosphates). The P-loops of the two structures overlay more closely than they do in the dTMP-ADP complex, although there are still main chain atom differences of 0.8 – 1.7 Å. The side chains of Asp^{17} (Asp^{15} in hTMPK) overlap but the carboxylates make different hydrogen bonding interactions, to Tyr^{107} in *Pf*TMPK, and to Arg^{97} in hTMPK. The P-loop arginine side chains are arranged much as they are in the dTMP-ADP complex, with the exception of the dual conformation of the side chain of Arg^{18} in *Pf*TMPK. The binding of AP_5dT clearly varies in detail between species, but is in keeping with the accepted mechanism of the enzyme.

*Pf*TMPK efficiently phosphorylates AZTMP

Another characteristic of *Pf*TMPK highlighted by the present kinetic studies is its ability to phosphorylate AZTMP 200-fold more efficiently than hTMPK (Table 2). The conversion of AZTMP to AZTDP by the human enzyme is a crucial step in the production of the active drug AZTTP in anti-viral therapy. The anti-viral effect of the drug is achieved by its inhibition of nascent DNA chain growth during replication following its acceptance as a substrate by the viral DNA polymerase [8].

Analysis of the PfTMPK-AZTMP-ADP complex shows that both nucleotide substrates are at full occupancy in each protomer in the asymmetric unit, however only in molecule A can the position of the azide group be defined with confidence (Figure 3c). The absence of electron density for azide in the other two protomers may reflect inherent disorder and is exacerbated by the modest (3.0 Å) resolution. The AZTMP azide moiety in molecule A is accommodated in a cavity surrounded by the side chains of Asp^{17}, Leu^{59}, Glu^{151} and Glu^{154} (Figure 3d). It causes a small reorientation of the dTMP phosphate group and minor conformational changes in the side chains of Glu^{154} and Asp^{17}, the latter retaining its hydrogen bond to the side chain of Tyr^{107}. Owing to the limited resolution, metal ions were not modelled in this complex (Table 3). The structure superimposes very closely on the dTMP-ADP complex (rmsΔ 0.27 Å over 208 C_α atoms) and the positions of the two sets of nucleotide ligands are essentially identical.

Comparison with the structure of the equivalent human enzyme complex (PDB entry 1e99) shows differences in the P-loop organisation similar to those observed in the equivalent dTMP-ADP comparisons. The close proximity of the side chain of Asp^{17} to the AZTMP in *Pf*TMPK causes a reorientation of the azide group relative to that in the human complex. This reorientation does not appear to affect the availability of Asp^{17} for catalysis. Indeed, given that it is likely that no further P-loop changes are required for transition state formation in the *P. falciparum* enzyme (cf. the structure of *Pf*TMPK-AP_5dT) it would appear to have a mechanistic advantage over the human enzyme, in which P-loop movements toward the transition state would result in a steric clash with the azide group of AZTMP. These structural observations provide a likely explanation for the higher activity towards AZTMP of *Pf*TMPK relative to hTMPK (Table 2).

Poor AZTMP phosphorylation in the type I TMPKs (e.g. the yeast and human enzymes), which contain a basic residue in the P-loop has been proposed to be due to the azido moiety in AZTMP disrupting an important bidentate interaction between the 3′ hydroxyl group of TMP and the conserved P-loop carboxylic acid which results in a displacement of the P-loop [8]. This is in contrast to type II TMPKs such as the *E. coli* enzyme where the analogous interaction with the P-loop carboxylic acid residue is side-on, permitting small conformational changes to accommodate the azido group of AZTMP without affecting significantly the position of the P-loop. It has been proposed that the P-loop could influence the phosphoryl transfer rate of type I TMPKs in different ways [11]. First, by shifting the position of ATP relative to the acceptor, catalysis would be impaired. Secondly, movement of the P-loop upon binding of AZTMP would result in the mis-positioning of P-loop arginine involved in catalysis (Arg^{18} in *Pf*TMPK). Third, mis-positioning of the P-loop carboxylic acid residue, a strictly conserved amino acid within the TMPK family, may hinder catalysis [18]. The steric clash between the azide group and the P-loop as the latter closes over the substrate is not likely to occur in *Pf*TMPK since hydrogen bonding between Asp^{17} and Tyr^{107} places the P-loop in the fully closed position at an earlier stage in the reaction, causing the azide group to adopt a different orientation (Figure 3c) which should not interfere with catalysis. This significance of this tyrosine residue for AZTMP activation is supported by kinetic data on the hTMPK F105Y mutant [18, 33] which is much more tolerant of AZTMP than the wild-type enzyme (Table 2).

In summary, despite the overall conservation of sequence and structure in the nucleotide binding site of human and *P. falciparum* TMPK, it is apparent that there are a number of subtle but seemingly significant differences in the substrate and inhibitor specificities. These are highlighted by differences in the reaction catalysed by the two enzymes with dGMP and AZTMP, evidence to suggest that *P. falciparum* TMPK may indeed be exploited as a target for anti-malarial drug discovery.

ACKNOWLEDGEMENTS

The authors thank the ESRF for access to beamlines and support by staff during visits, and Marek Brzozowski for assistance with crystal mounting. We thank the Diamond Light Source staff for help with use of the I24 microfocus beam line during initial solution of the dGMP complex.

FUNDING

Financial support for this research came from the Plan Nacional (SAF2007-62596), the RICET FIS Network (RD06/0021), the Junta de Andalucía (CVI-199), the European Union (ANTIMAL contract no. LSHP-CT-2005-018834) and the Wellcome Trust (grant no. 066742/F/02/Z).

REFERENCES

1 Hu, C. M. and Chang, Z. F. (2007) Mitotic control of dTTP pool: a necessity or coincidence? J. Biomed. Sci. **14**, 491-497

2 Mathews, C. K. (2006) DNA precursor metabolism and genomic stability. FASEB J. **20**, 1300-1314

3 Lavie, A. and Konrad, M. (2004) Structural requirements for efficient phosphorylation of nucleotide analogs by human thymidylate kinase. Mini Rev. Med. Chem. **4**, 351-359

4 Solaroli, N., Johansson, M., Persoons, L., Balzarini, J. and Karlsson, A. (2008) Substrate specificity of feline and canine herpesvirus thymidine kinase. Antiviral Res. **79**, 128-132

5 Carnrot, C., Wang, L., Topalis, D. and Eriksson, S. (2008) Mechanisms of substrate selectivity for *Bacillus anthracis* thymidylate kinase. Protein Sci. **17**, 1486-1493

6 Haouz, A., Vanheusden, V., Munier-Lehmann, H., Froeyen, M., Herdewijn, P., Van Calenbergh, S. and Delarue, M. (2003) Enzymatic and structural analysis of inhibitors designed against *Mycobacterium tuberculosis* thymidylate kinase: New insights into the phosphoryl transfer mechanism. J. Biol. Chem. **278**, 4963-4971

7 Lavie, A., Vetter, I. R., Konrad, M., Goody, R. S., Reinstein, J. and Schlichting, I. (1997) Structure of thymidylate kinase reveals the cause behind the limiting step in AZT activation. Nat. Struct. Biol. **4**, 601-604

8 Lavie, A., Ostermann, N., Brundiers, R., Goody, R. S., Reinstein, J., Konrad, M. and Schlichting, I. (1998) Structural basis for efficient phosphorylation of 3'-azidothymidine monophosphate by *Escherichia coli* thymidylate kinase. Proc. Natl Acad. Sci. U.S.A. **95**, 14045-14050

9 Kotaka, M., Dhaliwal, B., Ren, J., Nichols, C. E., Angell, R., Lockyer, M., Hawkins, A. R. and Stammers, D. K. (2006) Structures of *S. aureus* thymidylate kinase reveal an atypical active site configuration and an intermediate conformational state upon substrate binding. Protein Sci. **15**, 774-784

10 Li de la Sierra, I., Munier-Lehmann, H., Gilles, A. M., Barzu, O. and Delarue, M. (2001) X-ray structure of TMP kinase from *Mycobacterium tuberculosis* complexed with TMP at 1.95 Angstrom resolution. J. Mol. Biol. **311**, 87-100

11 Ostermann, N., Lavie, A., Padiyar, S., Brundiers, R., Veit, T., Reinstein, J., Goody, R. S., Konrad, M. and Schlichting, I. (2000) Potentiating AZT activation: Structures of wild-type and mutant Human thymidylate kinase suggest reasons for the mutants' improved kinetics with the HIV prodrug metabolite AZTMP. J. Mol. Biol. **304**, 43-53

12 Saraste, M., Sibbald, P. R. and Wittinghofer, A. (1990) The P-Loop - A common motif in ATP-binding and GTP-binding proteins. Trends Biochem. Sci. **15**, 430-434

13 Bone, R., Cheng, Y. C. and Wolfenden, R. (1986) Inhibition of adenosine and thymidylate kinases by bisubstrate analogs. J. Biol. Chem. **261**, 6410-6413

14 Lavie, A., Konrad, M., Brundiers, R., Goody, R. S., Schlichting, I. and Reinstein, J. (1998) Crystal structure of yeast thymidylate kinase complexed with the bisubstrate inhibitor P^1-(5'-adenosyl) P^5-(5'-thymidyl) pentaphosphate (TP_5A) at 2.0 Å resolution. Biochemistry **37**, 3677-3686

15 Ostermann, N., Schlichting, I., Brundiers, R., Konrad, M., Reinstein, J., Veit, T., Goody, R. S. and Lavie, A. (2000) Insights into the phosphoryltransfer mechanism of human thymidylate kinase gained from crystal structures of enzyme complexes along the reaction coordinate. Struct. Fold. Des. **8**, 629-642

16 Xiang Rong, S., Xia, L. and Xian Ming, P. (1999) An iso-random Bi Bi mechanism for adenylate kinase. J. Biol. Chem. **274**, 22238-22242

17 Schlichting, I. and Reinstein, J. (1997) Structures of active conformations of UMP kinase from *Dictyostelium discoideum* suggest phosphoryl transfer is associative. Biochemistry **36**, 9290-9296

18 Brundiers, R., Lavie, A., Veit, T., Reinstein, J., Schlichting, I., Ostermann, N., Goody, R. S. and Konrad, M. (1999) Modifying human thymidylate kinase to potentiate azidothymidine activation. J. Biol. Chem. **274**, 35289-35292

19 Kandeel, M. and Kitade, Y. (2008) Molecular characterization, heterologous expression and kinetic analysis of recombinant *Plasmodium falciparum* thymidylate kinase. J. Biochem. **144**, 245-250

20 Kandeel, M., Ando, T., Kitamura, Y., Abdel-Aziz, M. and Kitade, Y. (2009) Mutational, inhibitory and microcalorimetric analyses of *Plasmodium falciparum* TMP kinase. Implications for drug discovery. Parasitol. **136**, 11-25

21 Trager, W. and Jensen, J. B. (1976) Human malaria parasites in continuous culture. Science **193**, 673-675

22 Fang, J., Sullivan, M. and McCutchan, T. F. (2004) The effects of glucose concentration on the reciprocal regulation of rRNA promoters in *Plasmodium falciparum*. J. Biol. Chem. **279**, 720-725

23 Studier, F. W. (2005) Protein production by auto-induction in high-density shaking cultures. Prot. Express. Purif. **41**, 207-234

24 Bradford, M. M. (1976) Rapid and sensitive method for quantification of microgram quantities of protein utilizing principle of protein-dye binding. Anal. Biochem. **72**, 248-254

25 Blondin, C., Serina, L., Wiesmueller, L. and Gilles, A. M. (1994) Improved spectrophotometric assay of nucleoside monophosphate kinase activity using the pyruvate kinase/lactate dehydrogenase coupling system. Anal. Biochem. **220**, 219

26 Otwinowski, Z. and Minor, W. (1997) Processing of X-ray diffraction data collected in oscillation mode. In Macromolecular Crystallography, Pt A. pp. 307-326, Academic Press

27 McCoy, A. J., Grosse-Kunstleve, R. W., Adams, P. D., Winn, M. D., Storoni, L. C. and Read, R. J. (2007) Phaser crystallographic software. J. Appl. Crystallogr. **40**, 658-674

28 CCP4. (1994) The CCP4 Suite - Programs for protein crystallography. Acta Crystallogr. Sect. D Biol. Crystallogr. **50**, 760-763

29 Murshudov, G. N., Vagin, A. A. and Dodson, E. J. (1997) Refinement of macromolecular structures by the maximum-likelihood method. Acta Crystallogr. Sect. D Biol. Crystallogr. **53**, 240-255

30 Emsley, P. and Cowtan, K. (2004) Coot: model-building tools for molecular graphics. Acta Crystallogr. Sect. D Biol. Crystallogr. **60**, 2126-2132

31 Schuettelkopf, A. W. and van Aalten, D. M. F. (2004) PRODRG - a tool for high-throughput crystallography of protein-ligand complexes. Acta Crystallogr. Sect. D Biol. Crystallogr. **60**, 1355-1363.

32 Herzberg, O. and Moult, J. (1991) Analysis of the steric strain in the polypeptide backbone of protein molecules. Prot. Struct. Funct. Genet. **11**, 223-229

33 Wöhrl, B. M., Loubiere, L., Brundiers, R., Goody, R. S., Klatzmann, D. and Konrad, M. (2005) Expressing engineered thymidylate kinase variants in human cells to improve AZT phosphorylation and human immunodeficiency virus inhibition. J. Gen. Virol. **86,** 757-764

34 Topalis, D., Collinet, B., Gasse, C., Dugue, L., Balzarini, J., Pochet, S. and Deville-Bonne, D. (2005) Substrate specificity of vaccinia virus thymidylate kinase. FEBS J. **272**, 6254-6265

35 Su, J. Y. and Sclafani, R. A. (1991) Molecular cloning and expression of the human deoxythymidylate kinase gene in yeast. Nucl. acids Res. **19**, 823-827

36 Auvynet, C., Topalis, D., Caillat, C., Munier-Lehmann, H., Seclaman, E., Balzarini, J., Agrofoglio, L. A., Kaminski, P. A., Meyer, P., Deville-Bonne, D. and El Amri, C. (2009) Phosphorylation of dGMP analogs by vaccinia virus TMP kinase and human GMP kinase. Biochem. Biophys. Res. Commun. **388**, 6-11

37 Van Rompay, A. R., Johansson, M. and Karlsson, A. (2000) Phosphorylation of nucleosides and nucleoside analogs by mammalian nucleoside monophosphate kinases. Pharmacol. Therapeut. **87**, 189-198

38 Jong, A., Yeh, Y. and Ma, J. J. (1993) Characteristics, substrate analysis, and intracellular location of *Saccharomyces cerevisiae* UMP Kinase. Arch. Biochem. Biophys. **304**, 197-204

39 Kandeel, M., Kitamura, Y. and Kitade, Y. (2009) The exceptional properties of *Plasmodium* deoxyguanylate pathways as a potential area for metabolic and drug discovery studies. Nucl. Acids Symp. Ser. (Oxf), 39-40

40 Caillat, C., Topalis, D., Agrofoglio, L. A., Pochet, S., Balzarini, J., Deville-Bonne, D. and Meyer, P. (2008) Crystal structure of poxvirus thymidylate kinase: An unexpected dimerization has implications for antiviral therapy. Proc. Natl Acad. Sci. U.S.A. **105**, 16900-16905

41 Teplyakov, A., Sebastiao, P., Obmolova, G., Perrakis, A., Brush, G. S., Bessman, M. J. and Wilson, K. S. (1996) Crystal structure of bacteriophage T4 deoxynucleotide kinase with its substrates dGMP and ATP. EMBO J. **15**, 3487-3497

42 Gouet, P., Courcelle, E., Stuart, D. I. and Metoz, F. (1999) ESPript: analysis of multiple sequence alignments in PostScript. Bioinform. **15**, 305-308

43 Potterton, L., McNicholas, S., Krissinel, E., Gruber, J., Cowtan, K., Emsley, P., Murshudov, G. N., Cohen, S., Perrakis, A. and Noble, M. (2004) Developments in the CCP4 molecular-graphics project. Acta Crystallogr. Sect. D Biol. Crystallogr. **60**, 2288-2294

FIGURE LEGENDS

Figure 1.

(a) Structure-based amino acid sequence alignment of selected TMPK proteins (Pf, *Plasmodium falciparum*; Hu, human; Sc, *Saccharomyces cerevisiae*; Mt, *Mycobacterium tuberculosis*; Ec, *Escherichia coli*). Strictly conserved residues are coloured red and well-conserved residues are coloured yellow. The locations of the P-loop, critical loop and lid region in the *P. falciparum* enzyme are highlighted by red triangles, red stars and a blue bar, respectively. The secondary structure elements of *Pf*TMPK are shown above the sequence alignment. This figure was generated using ESPript [42].

(b) Stereo view of protomer A of *Pf*TMPK-TMP-ADP (ribbon) showing the dTMP substrate and ADP product as spheres, the P-loop (red), lid region (green), the critical loop (magenta) and two sodium ions (I and II, grey spheres). Structure figures were made with CCP4mg [43].

Figure 2.

(a) The dTMP binding site in the *Pf*TMPK dTMP-ADP complex (protein and solvent coloured blue, dTMP by atom type) superimposed on the equivalent human complex (pdb code 1e2d, yellow).

(b) The ADP binding site. The position of the ADP base is displaced somewhat, due to shifts in the lid and P-loops, the more tightly closed *Pf*TMPK structure perhaps reflecting the binding of sodium ions.

(c) Superposition of magnesium and sodium ions in the human (yellow ribbon) and *Pf*TMPK complexes (blue) respectively, with associated $2F_o$-F_c electron density contoured at 1σ. Sodium ions are shown as grey spheres, magnesium ions in black and water molecules in red.

Figure 3.

(a) Stereo view of the binding of dGMP in the dGMP-ADP complex coloured by atom, with the main chain shown as a transparent blue ribbon. Superimposed on this are the *Pf*TMPK-dTMP complex, (dTMP coloured red, protein side chains coral) and the human dTMP complex (protein side chains yellow, ligand omitted for clarity).

(b) Stereo view of the binding of the bisubstrate inhibitor AP_5dT in the *Pf*TMPK-TMP-AP_5dT complex (coloured by atom). The *Pf*TMPK main chain is shown as a transparent blue ribbon, and ligand-interacting side chains in ball and stick. Sodium ions (I and II) are shown as grey spheres; water molecules are red. Hydrogen bonding interactions are represented by dashed lines. Also shown are the same ligand in complexes for other species: human (1e2g, black), yeast (3tmk, coral) and *E. coli* (4tmk, blue). The Mg(I) ion from the human AP_5dT-ADP complex is shown as a black sphere, the position of a second magnesium, Mg(II) is taken from the human TMP complex (1e2d).

(c) Stereo view of protomer A of the *Pf*TMPK-AZTMP complex (ligands and side chains coloured by atom type, blue ribbon for main chain). There is electron density, albeit at a low level, to indicate the position of the azide in this protomer, but not in the other two molecules in the asymmetric unit. The AZTMP from the human complex is superimposed (yellow).

(d) Electrostatic surface around the ligand in the *Pf*TMPK-AZTMP complex showing how it is accommodated in the binding site.

Biochemical Journal Immediate Publication. Published on 30 Mar 2010 as manuscript BJ20091880

Table 1. Kinetic parameters for *Plasmodium falciparum* TMPK

Values obtained in this study were compared to parameters previously reported [20].

Substrate	k_{cat} (s^{-1})	K_m (μM)	k_{cat}/K_m (s^{-1} mM^{-1})	k_{cat}/K_m (s^{-1} mM^{-1}) [20]
dTMP	4.9 ± 0.1	10.7 ± 0.5	458	154
AzTMP	1.8 ± 0.04	9.1 ± 0.5	198	-
dGMP	4.7 ± 0.2	12.6 ± 0.6	373	94
dUMP	6.2 ± 0.4	155 ± 10	40	5.2
5FdUMP	11.3 ± 0.3	47 ± 4.5	240	-
dIMP	3.0 ± 0.07	349 ± 25	9	0.77
GMP	0.30 ± 0.01	253 ± 24	1	-

Table 2. Kinetic parameters of TMPKs from different organisms for dTMP and AZTMP

Organism	k_{cat} (s^{-1}) dTMP	K_m (μM) dTMP	k_{cat}/K_m (s^{-1} mM^{-1})	k_{cat} (s^{-1}) AZTMP	K_m (μM) AZTMP	k_{cat}/K_m (s^{-1} mM^{-1})	Ratio k_{cat}/K_m dTMP/AZTMP
E. coli [a]	15	2.7	5555	6	30	200	28
S. cerevisiae [a]	35	9	3889	0.175	6	29	134
P. falciparum	4.9	10.7	458	1.8	9.1	198	2.3
H. sapiens, WT [b]	0.73	6.3	116	0.012	12	1	116
H. sapiens, F105Y [b]	0.17	4.2	40	0.25	3.8	66	0.6

[a] From reference [14]

[b] From reference [18]

Table 3. Data processing and refinement statistics for the *Pf*TMPK complexes

Protein complex	**dTMP-ADP**	**AP_5dT**	**AZTMP-ADP**	**dGMP-ADP**
ESRF beamline / wavelength (Å)	ID23-1 / 0.9184	ID14-4 / 0.9765	ID14-4 / 0.9395	ID23-1 / 0.976
Data Collection Statistics				
Resolution limits [a] (Å)	40.0 – 1.90 (1.93 – 1.90)	40.0 – 2.70 (2.80 – 2.70)	40.0 – 3.00 (3.11 – 3.00)	50.0 – 2.4 (2.49 – 2.40)
$P3_121$ cell dimensions (Å)	*a* = 110.13 *c* = 120.10	*a* = 109.54 *c* = 119.35	*a* = 110.34 *c* = 119.11	*a* = 110.74 *c* = 119.36
Number of unique reflections	67,190	23,265	17,385	33,557
Completeness [a] (%)	94.3 (47.4)	99.2 (92.4)	99.9 (99.9)	100.0 (100.0)
Multiplicity [a]	5.1 (2.0)	8.1 (3.7)	9.4 (5.6)	10.9 (10.4)
R-merge [a]	0.083 (0.298)	0.121 (0.489)	0.115 (0.287)	0.150 (0.944)
I/σI [a]	17.4 (2.2)	16.8 (1.7)	22.6 (5.0)	18.3 (3.3)
Refinement Statistics				
R-cryst / *R*-free (%)	17.33 / 20.50	18.03 / 26.94	19.34 / 28.69	20.09 / 26.03
rmsΔ bond lengths (Å) [b]	0.012 (0.022)	0.021 (0.022)	0.020 (0.022)	0.014 (0.020)
rmsΔ angles (º) [b]	1.365 (1.979)	2.217 (1.977)	2.166 (1.972)	1.486 (1.922)
rmsΔ chiral volume ($Å^3$) [b]	0.091 (0.200)	0.130 (0.200)	0.137 (0.200)	0.108 (0.200)
Ramachandran outliers (%)	1.8	1.8	4.5	1.6
$B_{average}$ on all atoms ($Å^2$)	19.3	39.0	31.8	43.5

[a] Highest resolution shell statistics given in parentheses

[b] Average ideal values given in parentheses.

Biochemical Journal Immediate Publication. Published on 30 Mar 2010 as manuscript BJ20091880

1a

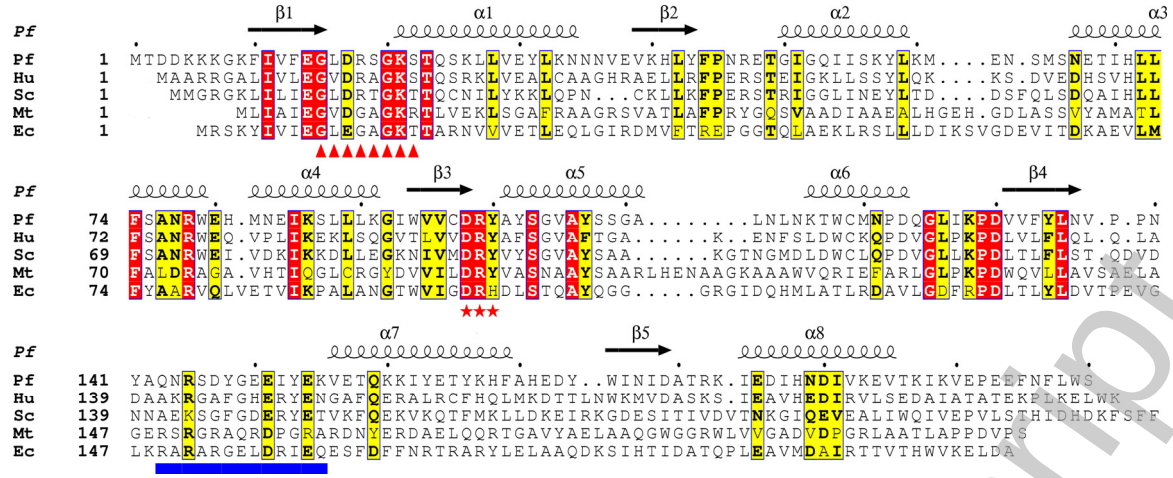

1b

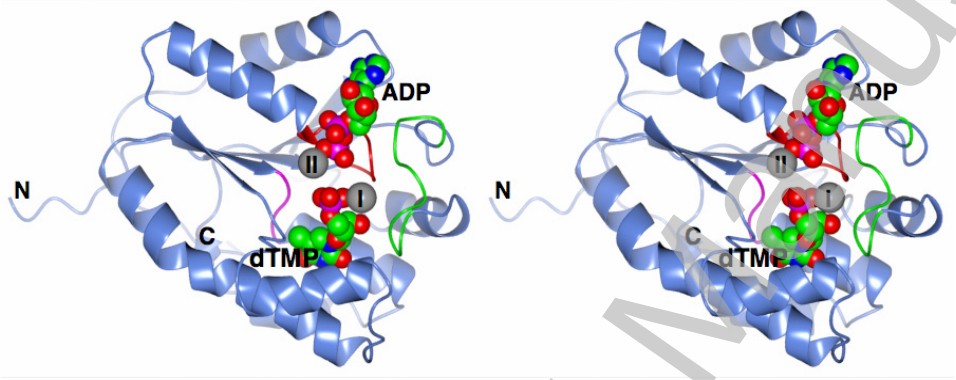

2a

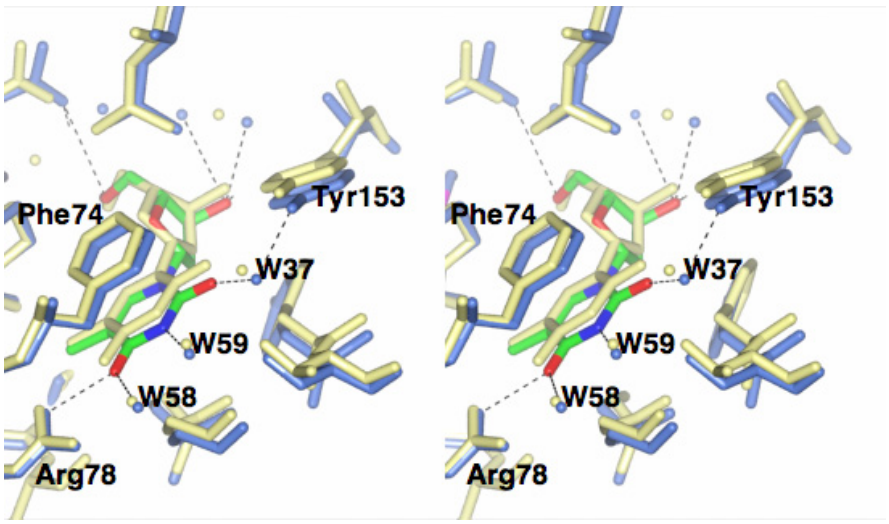

2b

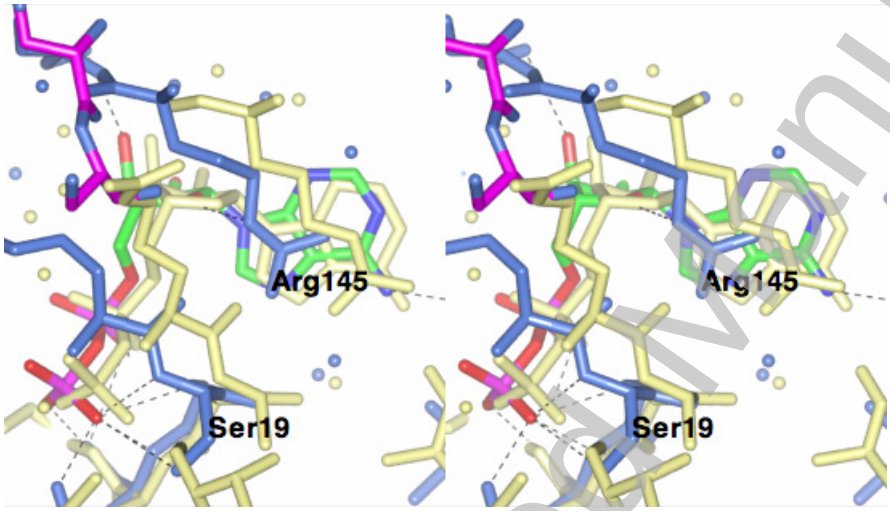

2c

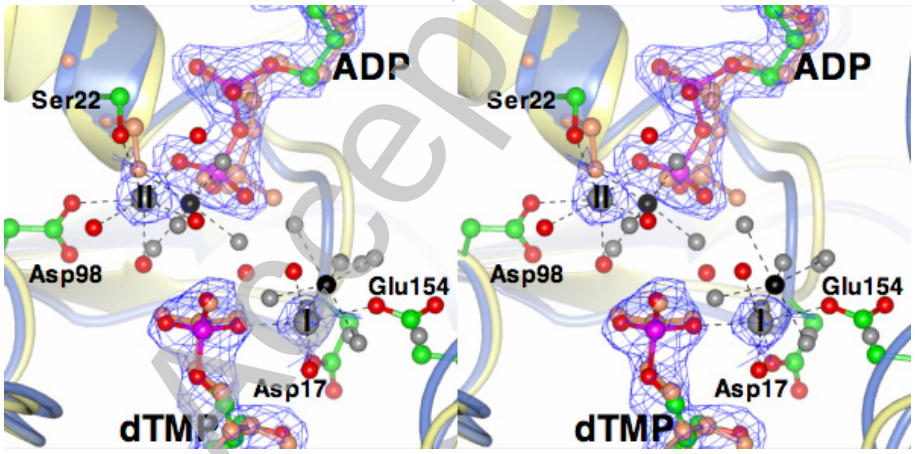

3a

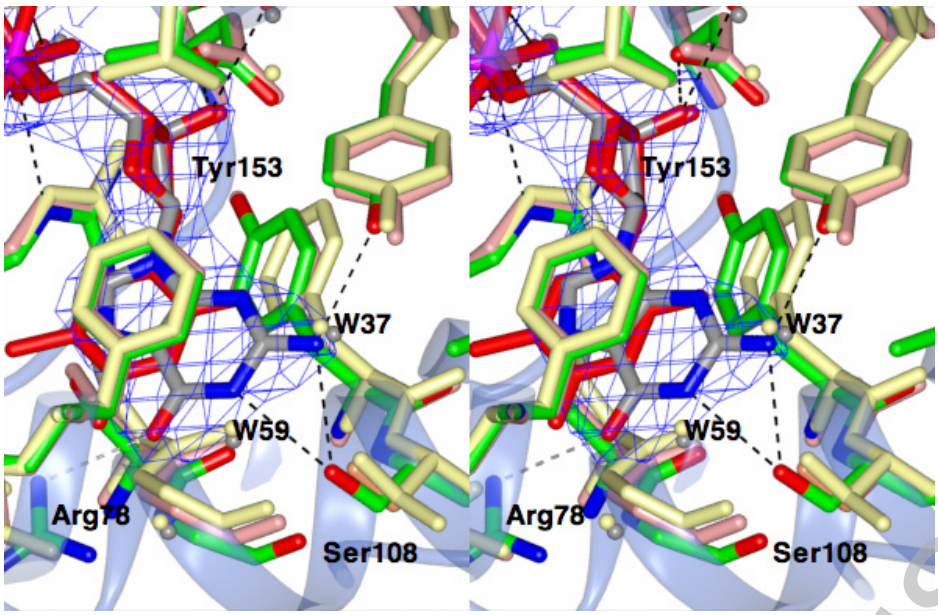

3b

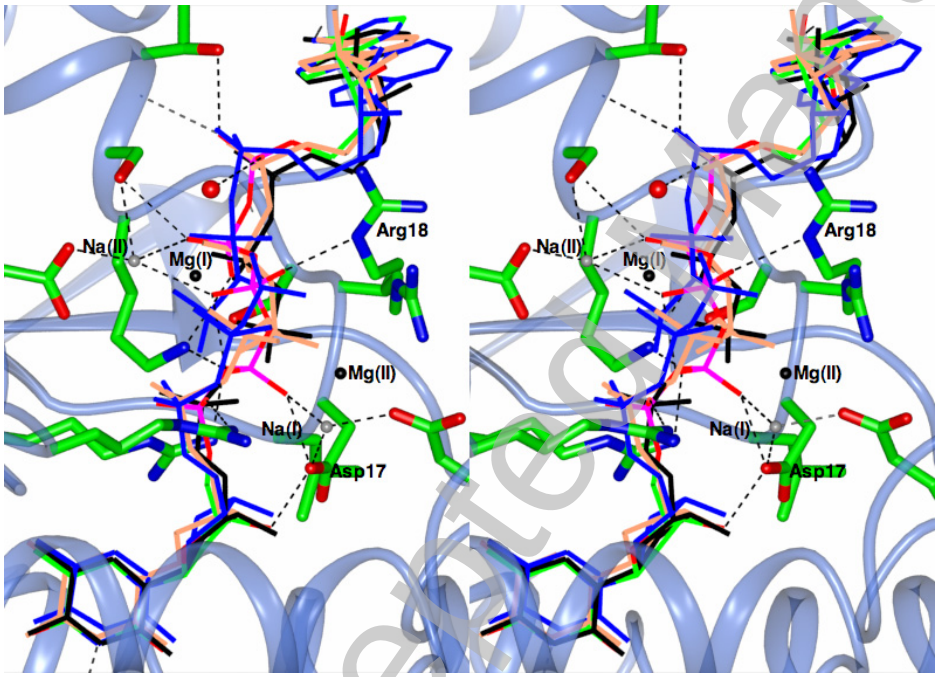

3c

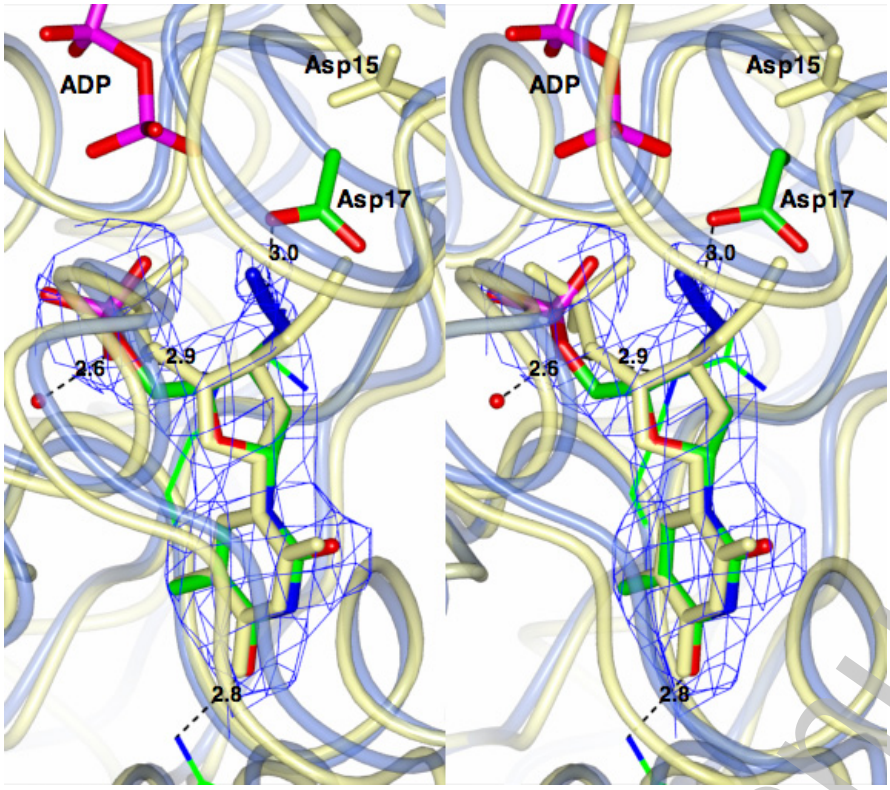

3d